Multimode Quasinormal Spectrum from a Perturbed Black Hole

Collin D. Capano,[1,2,3] Miriam Cabero,[4] Julian Westerweck,[1,2] Jahed Abedi,[1,2,5] Shilpa Kastha,[6,1,2] Alexander H. Nitz,[1,2] Yi-Fan Wang,[1,2] Alex B. Nielsen,[5] and Badri Krishnan[1,2,7]

[1]*Max-Planck-Institut für Gravitationsphysik (Albert-Einstein-Institut), Callinstraße 38, 30167 Hannover, Germany*
[2]*Leibniz Universität Hannover, 30167 Hannover, Germany*
[3]*Department of Physics, University of Massachusetts, Dartmouth, Massachusetts 02747, USA*
[4]*Department of Physics and Astronomy, The University of British Columbia, Vancouver BC V6T 1Z4, Canada*
[5]*Department of Mathematics and Physics, University of Stavanger, NO-4036 Stavanger, Norway*
[6]*Niels Bohr International Academy, Niels Bohr Institute, Blegdamsvej 17, 2100 Copenhagen, Denmark*
[7]*Institute for Mathematics, Astrophysics, and Particle Physics, Radboud University, Heyendaalseweg 135, 6525 AJ Nijmegen, The Netherlands*

(Received 16 June 2023; revised 25 August 2023; accepted 5 October 2023; published 28 November 2023)

When two black holes merge, the late stage of gravitational wave emission is a superposition of exponentially damped sinusoids. According to the black hole no-hair theorem, this ringdown spectrum depends only on the mass and angular momentum of the final black hole. An observation of more than one ringdown mode can test this fundamental prediction of general relativity. Here, we provide strong observational evidence for a multimode black hole ringdown spectrum using the gravitational wave event GW190521, with a maximum Bayes factor of 56 ± 1 (1σ uncertainty) preferring two fundamental modes over one. The dominant mode is the $\ell = m = 2$ harmonic, and the subdominant mode corresponds to the $\ell = m = 3$ harmonic. The amplitude of this mode relative to the dominant harmonic is estimated to be $A_{330}/A_{220} = 0.2^{+0.2}_{-0.1}$. We estimate the redshifted mass and dimensionless spin of the final black hole as $330^{+30}_{-40} M_\odot$ and $0.86^{+0.06}_{-0.11}$, respectively. We find that the final black hole is consistent with the no-hair theorem and constrain the fractional deviation from general relativity of the subdominant mode's frequency to be $-0.01^{+0.08}_{-0.09}$.

DOI: 10.1103/PhysRevLett.131.221402

Introduction.—A perturbed black hole approaches equilibrium by emitting a spectrum of damped sinusoidal gravitational-wave signals [1–3]. Unlike other astrophysical objects, the ringdown spectrum of a black hole is remarkably simple. General relativity predicts that the frequencies and damping times of the entire spectrum of damped sinusoids, or "quasinormal modes," are fully determined by just two numbers: the black hole mass M and angular momentum J, as described by the Kerr solution [4]. This prediction, a consequence of the black hole "no-hair theorem," does not hold in many alternate theories [5]. If astrophysical black holes are observed to violate this property, it indicates new physics beyond standard general relativity.

In order to observationally test this prediction using binary black hole mergers, an important observational challenge must be met: at least two ringdown modes must be observed [6]. The higher the binary mass ratio asymmetry, the more likely it is that subdominant ringdown modes are observable. However, more asymmetric binary systems are less likely to be formed, and also lead to weaker signals. Population studies suggested that such multimode ringdown modes were unlikely to be observed until the next generation of gravitational-wave observatories [7,8], since black hole population models did not anticipate observations of massive, asymmetric binaries.

Here, we confound this expectation with the gravitational-wave event GW190521, detected by the two LIGO detectors and Virgo at 03:02:29 UTC on May 21, 2019 [9,10]. This is the heaviest confidently detected black hole merger event observed to date [11,12]. The signal is consistent with the merger of two high mass black holes that merge at a low frequency relative to the detector sensitivity band. As such, it has a barely observable inspiral; the signal is dominated by the merger and ringdown phase.

GW190521 was initially reported as the merger of two comparable mass black holes [9,10]. If the spins are aligned, one would not expect to detect subdominant ringdown modes. However, there was significant posterior

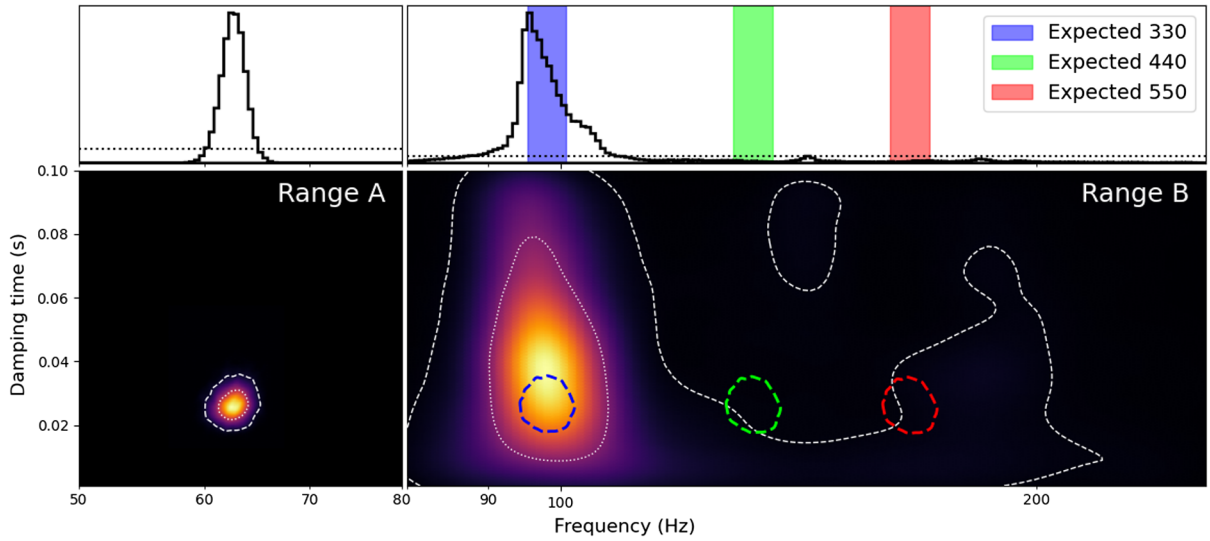

FIG. 1. Marginal posterior probability distributions on frequency and damping time from an agnostic quasinormal mode analysis of GW190521 at 6 ms after $t_{\rm ref}$. A single mode is searched for in each of the shown frequency ranges, range A (50–80 Hz) and range B (80–256 Hz). Top panels show the marginal posterior on the mode frequencies, with priors indicated by dotted lines. White dotted (dashed) contours in the bottom panels show the 50th (90th) credible regions. Assuming the dominant mode in range A corresponds to the (220) mode of a Kerr black hole, we estimate what the frequency and damping times would be of the (330), (440), and (550) modes (blue, green, and red regions, respectively). The mode in range B is clearly consistent with the expected frequency and damping time of the (330) mode. Here, we do not see the (440) and (550) modes, indicating they are weaker than the (330) mode. This is consistent with an asymmetric binary black hole merger.

support for precession in GW190521. Furthermore, subsequent reanalysis of the data found that the progenitor masses could have been unequal [13,14]. Both of these scenarios suggest the possibility of detectable subdominant modes [15,16]. Here, we find strong evidence for multimode damped sinusoids in the ringdown phase of the gravitational wave event GW190521.

Multimode agnostic search.—A quasinormal mode description of the gravitational wave from a binary black hole is not expected to be valid until after the binary has merged to form a perturbed black hole. On the flip side, the damping time of an $O(100M_\odot)$ black hole is $O(10\ \mathrm{ms})$, leaving a window of only a few tens of milliseconds after merger in which the ringdown is detectable above noise. Accurate identification of the merger time is therefore crucial to extract quasinormal modes from the data. To account for uncertainty in the merger time of GW190521 due to modeling systematics, we perform a series of analyses in short time increments starting at a geocentric Global Positioning System reference time $t_{\rm ref} = 1\,242\,442\,967.445$. This time is taken from the maximum likelihood merger time obtained via the analysis in Nitz and Capano [13]. We also fix the sky location to the maximum likelihood values from the same analysis.

The ringdown spectrum of a Kerr black hole consists of an infinite set of frequencies $f_{\ell mn}$ and damping times $\tau_{\ell mn}$ labeled by three integers (ℓ, m, n). Here, ℓ and m are the usual angular harmonic numbers. The third index $n \geq 0$ denotes overtones, with $n = 0$ being the fundamental mode. The most agnostic way to search for quasinormal modes from a perturbed black hole is to search for them individually, without assuming any relation between them. Such a search is complicated by the nature of quasinormal modes: they are not orthogonal, meaning that modes that overlap in time must be sufficiently separated in frequency or damping time in order to be distinguishable. Simulations of binary black hole mergers have shown that the fundamental $\ell = m = 2$ mode is typically significantly louder than other modes. In order to extract subdominant modes from noisy data in an agnostic search it is useful to separate the dominant mode in frequency from the others.

A visual inspection of the time- and frequency-domain data taken at the reference time revealed significant power in the two LIGO detectors between 60 and 70 Hz (see the Supplemental Material [17]). In order to isolate this and search for subdominant modes we constructed three frequency ranges: "range A," 50–80 Hz; "range B," 80–256 Hz, and "range C," 15–50 Hz. We search for one quasinormal mode in each range using Bayesian inference. We use uniform priors on the relative amplitudes of the modes in range B and C between 0 and 0.9 times the mode in range A. No other relation is assumed between the modes.

We repeat this analysis at time steps of $t_{\rm ref} + 0$, 6, 12, 18, and 24 ms. As expected from the visual inspection of the data, we find a significant mode in range A at all grid points, which decreases in amplitude at later times. A clear second mode is found in range B. This mode is most visible at $t_{\rm ref} + 6$ ms, the result of which is shown in Fig. 1 (results at other times are shown in the Supplemental Material). The frequency of the secondary mode at this time is 98^{+89}_{-7} Hz with a damping time of 40^{+50}_{-30} ms, while the primary mode

has a frequency of 63^{+2}_{-2} Hz and damping time 26^{+8}_{-6} ms. The signal-to-noise ratio (SNR) of the primary and secondary modes of the maximum likelihood waveform is 12.2 and 4.1, respectively. Results from range C (not shown) are consistent with noise.

The dominant mode found at 63^{+2}_{-2} Hz is expected to be the quadrupolar $\ell = m = 2, n = 0$ fundamental mode. Measurement of f_{220} and τ_{220} provides an estimate of the mass and angular momentum of the remnant black hole [30]. This in turn predicts the entire ringdown spectrum of subdominant modes. Figure 1 shows that the subdominant mode at 98^{+89}_{-7} Hz is consistent with the $\ell = m = 3, n = 0$ mode. This is also in agreement with expectations from numerical simulations of binary black hole mergers [15,31,32].

To quantify the agreement between the expected (330) mode and the observed mode in range B, we multiply the observed posterior in range B (color map in Fig. 1) with the expected distribution using range A (indicated by the blue contour in Fig. 1) and integrate [33]. This yields a statistic ζ that is proportionate to the agreement between the expected mode and the observed mode. Repeating on all the grid points, we find that ζ obtains a maximum value of 1.27 at $t_{\rm ref} + 6$ ms, consistent with our visual inspection. In Ref. [33] we perform a large simulation campaign in the data surrounding GW190521. Repeating the agnostic analysis on these simulations, we find that the probability of finding $\zeta \geq 1.27$ in noise is ~0.004.

Consistency with the Kerr solution.—The search for damped sinusoids in the previous section assumed no particular relation between different modes, with a corresponding large prior parameter volume. In this section, we assume that the frequency and damping times of the damped sinusoids are related as in the ringdown of a Kerr black hole. This reduces the prior parameter volume and focuses in on particular modes. The amplitudes and phases of the modes are left as free parameters, since they depend on the specific initial state of the remnant black hole immediately after the merger.

For this analysis, we model the ringdown signal based on the final Kerr black hole mass, M_f, and dimensionless spin, $\chi_f = J_f/M_f^2$. We expect only a subset of the entire spectrum of quasinormal modes to be visible above noise. Including all possible modes in our signal model can lead to overfitting the data. For this reason we perform several analyses, which include different combinations of the (330), (440), (210), and (550) modes, in addition to the dominant (220) mode. Numerical simulations of binary black hole mergers have generally shown these modes to be the strongest [32]. Giesler *et al.* [34] showed that including overtones of the dominant harmonic allows a quasinormal mode description of the signal to be used at earlier times, close to merger. We therefore also perform analyses in which we include the first overtone of the dominant harmonic $(\ell mn) = (221)$. We use a prior range on the (330) amplitude of $[0, 0.5]A_{220}$, while for the (221) mode we use $[0, 5]A_{220}$; prior ranges for the other modes can be found in the data release accompanying this Letter. These choices for the amplitude priors are sufficiently broad that they comfortably include results from numerical simulations [32,34]. Other prior choices are possible, e.g., a broader amplitude prior was adopted in Ref. [35].

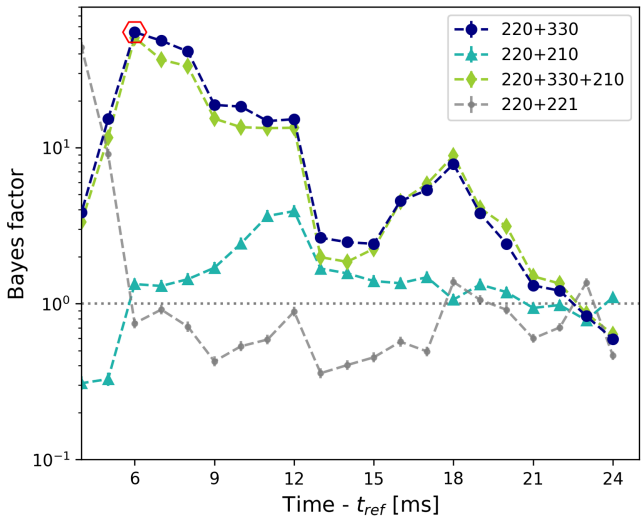

FIG. 2. Bayes factor of Kerr models that include the indicated modes. The Bayes factor for the $(220) + (221)$ model is calculated against the (220)-only model. For all other models, the Bayes factors are calculated by comparing the evidence for the model against the maximum of the (220)-only model and the $(220) + (221)$ model. The hexagon marks the point with the largest overall Bayes factor, which is for the $(220) + (330)$ model. Quoted mass and spin estimates are taken at this point, as well as the no-hair test described in the text.

We repeat these analyses in 1 ms intervals between $t_{\rm ref} + [-9\ {\rm ms}, 24\ {\rm ms}]$. We use Bayes factors to determine which model is most favored at each time step. For the model that includes the fundamental dominant harmonic (220) and its overtone (221), the Bayes factor is evaluated against the model with only the (220) mode. For models that include the (330) (or other subdominant modes), the Bayes factor is evaluated against the stronger of the (220) or (220) + (221) models.

The Bayes factors for the various multimode Kerr models are shown in Fig. 2. Consistent with the agnostic results, we find strong evidence for the presence of the (330) mode, with the Bayes factor for the $(220) + (330)$ model peaking at 56 ± 1 at $t_{\rm ref} + 6$ ms. The marginal posterior on the (330) amplitude is peaked away from zero at this time with a value of $A_{330}/A_{220} = 0.2^{+0.2}_{-0.1}$; see Fig. 3. The maximum likelihood ringdown waveforms at this time are shown in the Supplemental Material.

A Bayes factor of ~50 should correspond to a false alarm probability of 0.02. In Ref. [33] we validate this by repeating the analysis on a large number of simulated signals added to off-source data surrounding GW190521. There, we find that the distribution of Bayes factors in noise

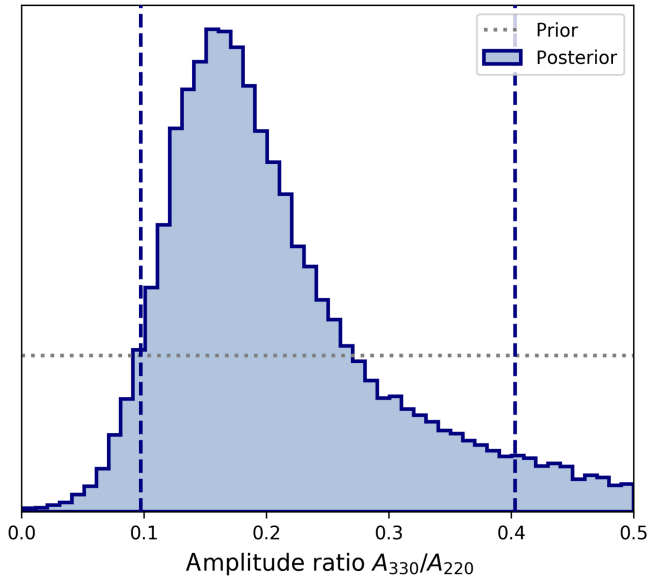

FIG. 3. Marginal posterior distribution of the amplitude ratio of the (330) mode relative to the (220) mode, A_{330}/A_{220}. The gray dotted line shows the prior, which was uniform in [0, 0.5). Vertical dashed lines indicate the 90% credible interval. The posterior distribution is obtained from the $(220)+(330)$ model starting at $t_{\rm ref}+6$ ms (red hexagon in Fig. 2), which is the most favored model in the Kerr analysis.

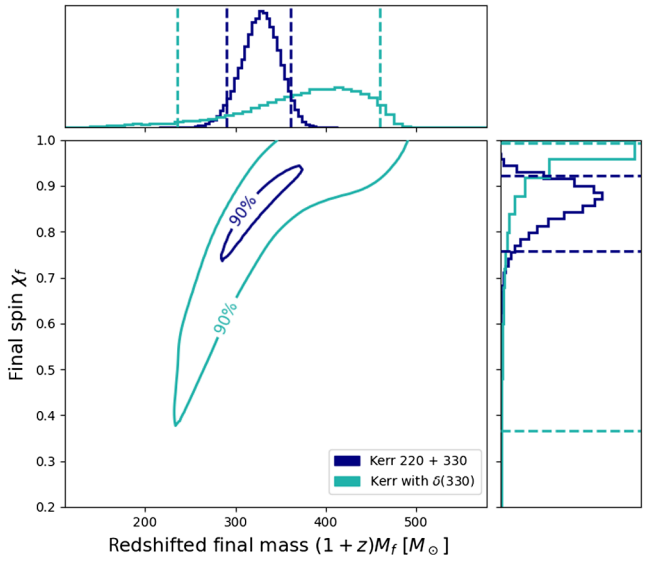

FIG. 4. Posterior distribution of final redshifted mass $(1+z)M_f$ and dimensionless spin χ_f measured at 6 ms after $t_{\rm ref}$ assuming the identified modes are the (220) and (330) modes of a Kerr black hole. Dashed lines indicate the 90% credible interval. For the Kerr with $\delta(330)$ results, we use fitting formulae [30] to convert the frequency $f_{330}(1+\delta f_{330})$ and damping time $\tau_{330}(1+\delta\tau_{330})$ into mass and spin.

matches expectations; e.g., the probability of obtaining a maximized Bayes factor as large as 56 from noise is ∼0.02. Our quoted Bayes factor is therefore robust against background noise fluctuations.

As can be seen in Fig. 2, the model that includes the (220), (330), and (210) modes is nearly as strong as the model with just the (220) and (330) mode in it, and is slightly favored at $t_{\rm ref}+18$ ms, indicating some support for the presence of the (210) mode in addition to the (330). However, the ratio of evidences between the $(220)+(330)$ and the $(220)+(330)+(210)$ models is order unity, i.e., the data is uninformative as to whether the (210) mode is observable *in addition to* the (330). A model consisting of just the (220) and (210) is disfavored at all times compared to any involving the (330), as can be seen in Fig. 2. We therefore only claim detection of the (330) mode, and make no claim regarding the observability of the (210) mode.

Figure 4 shows the redshifted mass and the dimensionless spin of the final black hole, measured with the $(220)+(330)$ Kerr model at 6 ms after $t_{\rm ref}$. We find that the remnant black hole has a redshifted mass $(1+z)M_f=330^{+30}_{-40}M_\odot$ and dimensionless spin $\chi_f=0.86^{+0.06}_{-0.11}$.

If a quasinormal model without overtones is used too close to merger, the resulting final mass estimate can be biased toward larger values [3,34]. We find the final mass estimate to be stable between 6 and 12 ms using the $(220)+(330)$ model (see the Supplemental Material for plot). This indicates that by this time the black hole has reached a regime of constant ringdown frequency—a requirement for the validity of linear-regime, quasinormal modes.

Given the strong evidence for the presence of the (330) mode at $t_{\rm ref}+6$ ms, we can perform the classic no-hair theorem test [6] (see also Ref. [36] for a reformulation in terms of parametric deviations). Here, we keep the dependence of f_{220} and τ_{220} on (M_f,χ_f) as in the Kerr solution but introduce fractional deviations δf_{330} and $\delta\tau_{330}$ of f_{330} and τ_{330}, respectively. We find good agreement with general relativity. Figure 4 shows the Kerr black hole mass M_f and dimensionless spin χ_f associated to the (330) mode frequency $f_{330}(1+\delta f_{330})$ and damping time $\tau_{330}(1+\delta\tau_{330})$ measured at 6 ms after $t_{\rm ref}$. Plots of the posterior distributions on the fractional deviations are provided in the Supplemental Material. We constrain the fractional deviation from Kerr to $\delta f_{330}=-0.01^{+0.08}_{-0.09}$. The damping time is only weakly constrained, with $\delta\tau_{330}=0.6^{+1.9}_{-1.2}$.

Discussions and conclusions.—The redshifted final mass of GW190521 measured by the LIGO and Virgo Collaborations using a (220) ringdown fit was $(1+z)M_f=282.2^{+50.0}_{-61.9}M_\odot$, or $259.2^{+36.6}_{-29.0}M_\odot$ when analyzing the full signal [11]. The low-mass-ratio part of the posterior of Nitz and Capano [13] found $(1+z)M_f\sim 260M_\odot$ using the full signal [37,38]. These results are somewhat in tension with the final mass and spin inferred from the ringdown modes found here.

However, the complete waveform models used in the above analyses may not include all relevant physical

effects. This, coupled with the fact that GW190521 has a very short inspiral signal, can lead to systematic errors for parameter estimation. For example, the waveform models used in the LIGO and Virgo Collaborations' analysis and Nitz and Capano assume quasicircular orbits, but several studies have indicated that the binary may have been eccentric at merger [39–41]. These studies have also found slightly larger estimates for the binary's total mass, making them more consistent with our estimate for the final mass. Even without eccentricity, the reanalysis in Estelles *et al.* [14] using a recalibrated time-domain model found a bimodal distribution for the final mass and spin. One of these modes yields similar estimates for the mass and spin as we obtain here; see Ref. [33] for a more detailed comparison.

The ringdown waveforms used in this Letter are simpler and more robust than full inspiral-merger-ringdown models for signals like GW190521, provided they are applied sufficiently late in the postmerger regime. This argument would tend to favor the estimates derived in this Letter for the total mass. Nevertheless, a full resolution of this tension is beyond the scope of this work.

Evidence for overtones of the (220) mode very close to merger were previously found for the events GW150914 [42] and GW190521_074359 [35] (not to be confused with GW190521), although the strength of the evidence for the overtone is disputed [43,44]. Black hole spectroscopy tests showed consistency with the Kerr hypothesis for these events [35,42]. However, the resulting constraints were weaker than what we find with the (330) mode here. Furthermore, while there is strong numerical evidence for the presence of ringdown overtones close to the merger [34], a number of theoretical questions remain as to the validity of a quasinormal description of the black hole close to merger [45–49].

The true nature of the gravitational wave event GW190521 has been the subject of much speculation [50–52]. The interpretation of GW190521 as a head-on collision of two highly spinning Proca stars [52] predicts the presence of a (200) mode [53]. We do not find evidence for such a mode. Additionally, the high-mass, multiple-mode ringdown signal observed here does not agree with the scenario of a very massive star collapsing to a black hole of mass $\sim 50 M_{\odot}$ and an unstable massive disk [54].

Expectations based on population models were that black hole ringdown signals with multiple modes were unlikely to be observed with the Advanced LIGO and Virgo detectors [7,8] (although those population models did not include massive binaries). However, Forteza et al. [15] predicted that for even moderately asymmetric binaries (with mass ratios $\gtrsim 1.2$), the (330) mode would be the best observable mode. They further predicted that the (330) mode's frequency could be constrained to the $\sim 10\%$ level if the ringdown SNR is $\gtrsim 8$. Our results are remarkably consistent with this prediction: we get a ringdown SNR for GW190521 of ~ 12, and we constrain the (330) frequency to be within $\sim 10\%$ of the expected value from general relativity.

In summary, we have shown that GW190521 displays a distinct subdominant mode and that this mode is consistent with the (330) ringdown mode of a Kerr black hole.

Posterior data samples and data necessary to reproduce the figures are available at [55]. The gravitational-wave data used in this work were obtained from the Gravitational Wave Open Science Center (GWOSC) [56]. All software used in this analysis is open source. Bayesian inference was performed with the PyCBC library [57]. Configuration files used to perform all analyses can be found at [55]. Spheroidal harmonics, Kerr frequencies, and Kerr damping times were generated using PYKERR [58].

The authors thank Ofek Birnholtz, Jose Luis Jaramillo, Reinhard Prix, Bruce Allen, Evan Goetz, Saul Teukolsky, Maximiliano Isi, Juan Calderón-Bustillo, Abhay Ashtekar, and Bangalore Sathyaprakash for useful discussions and Xisco Jiménez Forteza for a careful reading of this manuscript. We thank also the Atlas Computational Cluster team at the Albert Einstein Institute in Hanover for assistance. M. C. acknowledges funding from the Natural Sciences and Engineering Research Council of Canada (NSERC). This research has made use of data obtained from the Gravitational Wave Open Science Center [56], a service of LIGO Laboratory, the LIGO Scientific Collaboration and the Virgo Collaboration. LIGO Laboratory and Advanced LIGO are funded by the United States National Science Foundation (NSF) who also gratefully acknowledge the Science and Technology Facilities Council (STFC) of the United Kingdom, the Max-Planck-Society (MPS), and the State of Niedersachsen/Germany for support of the construction of Advanced LIGO and construction and operation of the GEO600 detector. Additional support for Advanced LIGO was provided by the Australian Research Council. Virgo is funded, through the European Gravitational Observatory (EGO), by the French Centre National de Recherche Scientifique (CNRS), the Italian Istituto Nazionale di Fisica Nucleare (INFN) and the Dutch Nikhef, with contributions by institutions from Belgium, Germany, Greece, Hungary, Ireland, Japan, Monaco, Poland, Portugal, and Spain.

[1] C. V. Vishveshwara, Scattering of gravitational radiation by a Schwarzschild black-hole, Nature (London) **227**, 936 (1970).

[2] S. Chandrasekhar and S. L. Detweiler, The quasi-normal modes of the Schwarzschild black hole, Proc. R. Soc. A **344**, 441 (1975).

[3] B. P. Abbott *et al.*, Tests of general relativity with GW150914, Phys. Rev. Lett. **116**, 221101 (2016); **121**, 129902(E) (2018).

[4] R. P. Kerr, Gravitational field of a spinning mass as an example of algebraically special metrics, Phys. Rev. Lett. **11**, 237 (1963).

[5] V. Cardoso and P. Pani, Testing the nature of dark compact objects: A status report, Living Rev. Relativity **22**, 4 (2019).

[6] O. Dreyer, B. Kelly, B. Krishnan, L. S. Finn, D. Garrison, and R. Lopez-Aleman, Black hole spectroscopy: Testing general relativity through gravitational wave observations, Classical Quantum Gravity **21**, 787 (2004).

[7] E. Berti, A. Sesana, E. Barausse, V. Cardoso, and K. Belczynski, Spectroscopy of Kerr black holes with Earth- and space-based interferometers, Phys. Rev. Lett. **117**, 101102 (2016).

[8] M. Cabero, J. Westerweck, C. D. Capano, S. Kumar, A. B. Nielsen, and B. Krishnan, Black hole spectroscopy in the next decade, Phys. Rev. D **101**, 064044 (2020).

[9] R. Abbott *et al.*, GW190521: A binary black hole merger with a total mass of $150M_{\odot}$, Phys. Rev. Lett. **125**, 101102 (2020).

[10] R. Abbott *et al.*, Properties and astrophysical Implications of the $150M_{\odot}$ binary black hole merger GW190521, Astrophys. J. Lett. **900**, L13 (2020).

[11] R. Abbott *et al.*, GWTC-2: Compact binary coalescences observed by LIGO and Virgo during the first half of the third observing run, Phys. Rev. X **11**, 021053 (2021).

[12] A. H. Nitz, C. D. Capano, S. Kumar, Yi-Fan Wang, S. Kastha, M. Schäfer, R. Dhurkunde, and M. Cabero, 3-OGC: Catalog of gravitational waves from compact-binary mergers, Astrophys. J. **922**, 76 (2021).

[13] A. H. Nitz and C. D. Capano, GW190521 may be an intermediate mass ratio inspiral, Astrophys. J. Lett. **907**, L9 (2021).

[14] H. Estellés, S. Husa, M. Colleoni, M. Mateu-Lucena, M. d. Planas, C. García-Quirós, D. Keitel, A. Ramos-Buades, A. K. Mehta, A. Buonanno *et al.*, A detailed analysis of GW190521 with phenomenological waveform models, Astrophys. J. **924**, 79 (2022).

[15] X. Jiménez Forteza, S. Bhagwat, P. Pani, and V. Ferrari, Spectroscopy of binary black hole ringdown using overtones and angular modes, Phys. Rev. D **102**, 044053 (2020).

[16] H. Siegel, M. Isi, and W. Farr, The ringdown of GW190521: Hints of multiple quasinormal modes with a precessional interpretation, Phys. Rev. D **108**, 064008 (2023).

[17] See Supplemental Material at http://link.aps.org/supplemental/10.1103/PhysRevLett.131.221402, which includes Refs. 18–29, for a derivation of the likelihood function, details on the signal model and analysis settings, and additional figures that further illustrate results from our analysis.

[18] S. A. Teukolsky, Rotating black holes—separable wave equations for gravitational and electromagnetic perturbations, Phys. Rev. Lett. **29**, 1114 (1972).

[19] E. W. Leaver, An analytic representation for the quasi normal modes of Kerr black holes, Proc. R. Soc. A **402**, 285 (1985).

[20] E. Berti, V. Cardoso, J. A. Gonzalez, U. Sperhake, M. Hannam, S. Husa, and B. Brugmann, Inspiral, merger and ringdown of unequal mass black hole binaries: A multipolar analysis, Phys. Rev. D **76**, 064034 (2007).

[21] R. Kass and A. E. Raftery, Bayes Factors, J. Am. Stat. Assoc. **90**, 773 (1995).

[22] R. M. Gray, Toeplitz and circulant matrices: A review, Found. Trends Commun. Inf. Theor. **2**, 155 (2006).

[23] L. S. Finn, Detection, measurement and gravitational radiation, Phys. Rev. D **46**, 5236 (1992).

[24] B. Allen, W. G. Anderson, P. R. Brady, D. A. Brown, and J. D. E. Creighton, FINDCHIRP: An algorithm for detection of gravitational waves from inspiraling compact binaries, Phys. Rev. D **85**, 122006 (2012).

[25] B. Zackay, T. Venumadhav, J. Roulet, L. Dai, and M. Zaldarriaga, Detecting gravitational waves in data with non-Gaussian noise, Phys. Rev. D **104**, 063034 (2021).

[26] P. Virtanen *et al.*, SciPy 1.0–Fundamental algorithms for scientific computing in PYTHON, Nat. Methods **17**, 261 (2020).

[27] C. R. Harris *et al.*, Array programming with NumPy, Nature (London) **585**, 357 (2020).

[28] C. M. Biwer, C. D. Capano, S. De, M. Cabero, D. A. Brown, A. H. Nitz, and V. Raymond, PyCBC Inference: A PYTHON-based parameter estimation toolkit for compact binary coalescence signals, Publ. Astron. Soc. Pac. **131**, 024503 (2019).

[29] J. S. Speagle, DYNESTY: A dynamic nested sampling package for estimating Bayesian posteriors and evidences, Mon. Not. R. Astron. Soc. **493**, 3132 (2020).

[30] E. Berti, V. Cardoso, and C. M. Will, On gravitational-wave spectroscopy of massive black holes with the space interferometer LISA, Phys. Rev. D **73**, 064030 (2006).

[31] I. Kamaretsos, M. Hannam, S. Husa, and B. S. Sathyaprakash, Black-hole hair loss: Learning about binary progenitors from ringdown signals, Phys. Rev. D **85**, 024018 (2012).

[32] S. Borhanian, K. G. Arun, H. P. Pfeiffer, and B. S. Sathyaprakash, Comparison of post-Newtonian mode amplitudes with numerical relativity simulations of binary black holes, Classical Quantum Gravity **37**, 065006 (2020).

[33] C. D. Capano, J. Abedi, S. Kastha, A. H. Nitz, J. Westerweck, Y. F. Wang, M. Cabero, A. B. Nielsen, and B. Krishnan, Statistical validation of the detection of a subdominant quasi-normal mode in GW190521, arXiv:2209.00640.

[34] M. Giesler, M. Isi, M. A. Scheel, and S. A. Teukolsky, Black hole ringdown: The importance of overtones, Phys. Rev. X **9**, 041060 (2019).

[35] R. Abbott *et al.*, Tests of general relativity with binary black holes from the second LIGO-Virgo gravitational-wave transient catalog, Phys. Rev. D **103**, 122002 (2021).

[36] S. Gossan, J. Veitch, and B. S. Sathyaprakash, Bayesian model selection for testing the no-hair theorem with black hole ringdowns, Phys. Rev. D **85**, 124056 (2012).

[37] V. Varma, S. E. Field, M. A. Scheel, J. Blackman, L. E. Kidder, and H. P. Pfeiffer, Surrogate model of hybridized numerical relativity binary black hole waveforms, Phys. Rev. D **99**, 064045 (2019).

[38] G. Pratten *et al.*, Let's twist again: Computationally efficient models for the dominant and sub-dominant harmonic modes of precessing binary black holes, Phys. Rev. D **103**, 104056 (2021).
[39] I. M. Romero-Shaw, P. D. Lasky, E. Thrane, and J. C. Bustillo, GW190521: Orbital eccentricity and signatures of dynamical formation in a binary black hole merger signal, Astrophys. J. Lett. **903**, L5 (2020).
[40] V. Gayathri, J. Healy, J. Lange, B. O'Brien, M. Szczepanczyk, I. Bartos, M. Campanelli, S. Klimenko, C. O. Lousto, and R. O'Shaughnessy, Eccentricity estimate for black hole mergers with numerical relativity simulations, Nat. Astron. **6**, 344 (2022).
[41] J. C. Bustillo, N. Sanchis-Gual, A. Torres-Forné, and J. A. Font, Confusing head-on collisions with precessing intermediate-mass binary black hole mergers, Phys. Rev. Lett. **126**, 201101 (2021).
[42] M. Isi, M. Giesler, W. M. Farr, M. A. Scheel, and S. A. Teukolsky, Testing the no-hair theorem with GW150914, Phys. Rev. Lett. **123**, 111102 (2019).
[43] M. Isi and W. M. Farr, Revisiting the ringdown of GW150914, arXiv:2202.02941.
[44] R. Cotesta, G. Carullo, E. Berti, and V. Cardoso, Analysis of ringdown overtones in GW150914, Phys. Rev. Lett. **129**, 111102 (2022).
[45] H. P. Nollert, About the significance of quasinormal modes of black holes, Phys. Rev. D **53**, 4397 (1996).
[46] H. P. Nollert and R. Price, Quantifying excitations of quasinormal mode systems, J. Math. Phys. (N.Y.) **40**, 980 (1999).
[47] J. L. Jaramillo, P. Macedo, and L. Al Sheikh, Pseudospectrum and black hole quasi-normal mode (in)stability, Phys. Rev. X **11**, 031003 (2021).
[48] R. G. Daghigh, M. D. Green, and J. C. Morey, Significance of black hole quasinormal modes: A closer look, Phys. Rev. D **101**, 104009 (2020).
[49] W. L. Qian, K. Lin, C. Y. Shao, B. Wang, and R. H. Yue, Asymptotical quasinormal mode spectrum for piecewise approximate effective potential, Phys. Rev. D **103**, 024019 (2021).
[50] J. Sakstein, D. Croon, S. D. McDermott, M. C. Straight, and E. J. Baxter, Beyond the standard model explanations of GW190521, Phys. Rev. Lett. **125**, 261105 (2020).
[51] M. Safarzadeh and Z. Haiman, Formation of GW190521 via gas accretion onto Population III stellar black hole remnants born in high-redshift minihalos, Astrophys. J. Lett. **903**, L21 (2020).
[52] J. C. Bustillo, N. Sanchis-Gual, A. Torres-Forne, J. A. Font, A. Vajpeyi, R. Smith, C. Herdeiro, E. Radu, and S. H. W. Leong, GW190521 as a merger of Proca stars: A potential new vector boson of 8.7×10^{-13} eV, Phys. Rev. Lett. **126**, 081101 (2021).
[53] C. Palenzuela, I. Olabarrieta, L. Lehner, and S. L. Liebling, Head-on collisions of boson stars, Phys. Rev. D **75**, 064005 (2007).
[54] M. Shibata, K. Kiuchi, S. Fujibayashi, and Y. Sekiguchi, Alternative possibility of GW190521: Gravitational waves from high-mass black hole-disk systems, Phys. Rev. D **103**, 063037 (2021).
[55] C. Capano, S. Kastha, M. Cabero, and Y. Wang, gwastro/BH-Spectroscopy-GW190521: Published data release (2023), 10.5281/zenodo.10056546.
[56] R. Abbott *et al.* Open data from the third observing run of LIGO, Virgo, KAGRA, and GEO, Astrophys. J. **267**, 29 (2023).
[57] A. Nitz *et al.*, gwastro/pycbc: v2.0.5 release of PyCBC (2022), 10.5281/zenodo.6912865.
[58] C. Capano, cdcapano/pykerr: v0.1.0 (2023), 10.5281/zenodo.10056495.